Physics Letters A 381 (2017) 3276–3281

Contents lists available at ScienceDirect

Physics Letters A

www.elsevier.com/locate/pla

Identifying different mechanisms in the control of a nitrogen–vacancy center system

Shouzhi Li [a,b], Ling Yang [a,b], Dewen Cao [a,b], Yaoxiong Wang [a,b], Feng Shuang [a,b,c], Fang Gao [a,*]

[a] Institute of Intelligent Machines, Chinese Academy of Sciences, Hefei 230031, China
[b] Department of Automation, University of Science and Technology of China, Hefei 230026, China
[c] Department of Mechanical Engineering, Anhui Polytechnic University, Wuhu 241000, China

ARTICLE INFO

Article history:
Received 16 May 2017
Received in revised form 12 July 2017
Accepted 14 August 2017
Available online 25 August 2017
Communicated by A. Eisfeld

Keywords:
Quantum pathway
Dressed states
NV center

ABSTRACT

The nitrogen–vacancy (NV) center system has shown great potential in quantum computing due to its long decoherence time at room temperature by encoding the qubit in dressed states [28]. The corresponding control mechanisms, which is expressed by the pathways linking the initial and target states, can be naturally investigated with the Hamiltonian-encoding and observable-decoding (HE–OD) method in the interaction adiabatic representation. This is proved by the fact that the mechanisms change slightly with different detunings, magnetic and driving field intensities, and the dominant pathway is always $|g\rangle \rightarrow |d\rangle \rightarrow |g\rangle$, with $|g\rangle$ and $|d\rangle$ as the first two lowest dressed states. Cases are different in the diabatic representation. The orders of dominant pathways increase the driving field intensities. Tendencies of quantum pathway amplitudes with driving fields, magnetic fields and detunings change at different conditions, which can be analyzed from the Dyson series. HE–OD analysis show that the two states $|g\rangle$ and $|d\rangle$ in the interaction adiabatic representation are preferable to be employed as a qubit than the state pair $|0\rangle$ and $|-1\rangle$ in the diabatic representation under the current Hamiltonian and parameters.

1. Introduction

How to achieve an optimal and effective control of quantum systems has always been a hot topic due to its wide and potential application [1–12]. The corresponding control mechanism analysis is important to understand the underlying physics and can give hints to improve the control effect. The Hamiltonian-encoding and observable-decoding (HE–OD) technique has provided such a feasible means, and expressed the mechanism in terms of different pathways linking the initial and target states [12–21]. In the experiment, a signal function is firstly encoded in the Hamiltonian in a specific manner, and then the information of pathways is extracted by decoding the resultant nonlinear distortion of the output signal.

Quantum computation requires good control of quantum qubits. The nitrogen–vacancy (NV) center is an important candidate of solid-state quantum computing because of its special nature [22], such as long decoherence time at room temperature [23], good scalability and microwave manipulation [24]. In this context, we will perform a mechanism analysis on the NV center system with HE–OD.

This paper is organized as follows. Section 2 introduces the HE–OD method for mechanism analysis and the two representations for the NV center system. Section 3 gives the results. The final conclusions are presented in Section 4.

2. Methodology

2.1. The HE–OD method

It is known that the state of a quantum system can be described by the Schrödinger equation

$$i\frac{d\,|\Psi\,(t)\rangle}{dt} = H\,|\Psi\,(t)\rangle\,. \tag{1}$$

The state $\Psi\,(t)$ at time t can be obtained from the propagator $U\,(t)$ and the initial state $|\Psi\,(0)\rangle$ as $|\Psi\,(t)\rangle = U\,(t)\,|\Psi\,(0)\rangle$. The time evolution of $U\,(t)$ satisfies

$$i\frac{dU\,(t)}{dt} = HU\,(t)\,. \tag{2}$$

Its Dyson expansion is

* Corresponding author.
E-mail address: gaofang@iim.ac.cn (F. Gao).

http://dx.doi.org/10.1016/j.physleta.2017.08.031
0375-9601/

$$U(t) = I + (-i)\int_0^t H(t_1)\,dt_1 + (-i)^2\int_0^t H(t_2)\int_0^{t_2} H(t_1)\,dt_1 dt_2 + \cdots. \quad (3)$$

The transition amplitude from the initial state $|a\rangle$ to the target state $|b\rangle$ is given by $\langle b|U(t)|a\rangle$. So the n-th order pathway $|a\rangle \to |l_1\rangle \to \cdots \to |l_{n-1}\rangle \to |b\rangle$ has the amplitude

$$U_{ba}^{n(l_1,\ldots,l_{n-1})}(t) = (-i)^n \int_0^t \langle b|H(t_n)|l_{n-1}\rangle \times \int_0^{t_n} \langle l_{n-1}|H(t_{n-1})|l_{n-2}\rangle \times \cdots \times \int_0^{t_2} \langle l_1|H(t_1)|a\rangle\, dt_1 dt_2 \cdots dt_n. \quad (4)$$

The HE–OD method introduces a dimensionless time-like variable s, and the Hamiltonian is encoded as $H(t) \to H(t,s)$, which leads to a distorted output signal $\langle b|U(t,s)|a\rangle$. Then the method tries to extract the desired pathway amplitudes from these signals. In practice, each element of the original Hamiltonian H is modulated as

$$H_{ij}(t) \to H_{ij}(t)\, m_{ij}(s).$$

Here the modulation function $m_{ij}(s)$ is taken to be the Fourier form

$$m_{ij}(s) = \exp\left(2\pi i \gamma_{ij} s/N\right), s = 1, 2, \cdots, N.$$

The propagator under the new Hamiltonian $H(t) \to H(t,s)$ evolves as

$$i\frac{dU(t,s)}{dt} = \begin{pmatrix} H_{11}(t)\,m_{11}(s) & \cdots & H_{1d}(t)\,m_{1d}(s) \\ \vdots & \vdots & \vdots \\ H_{d1}(t)\,m_{d1}(s) & \cdots & H_{dd}(t)\,m_{dd}(s) \end{pmatrix} U(t,s). \quad (5)$$

The transition amplitude from the initial state to the target state becomes

$$\langle b|U(t,s)|a\rangle = \sum_{n=1}^{\infty}\sum_{l_1,\cdots,l_{n-1}=1}^{d} U_{ba}^{n(l_1,\ldots,l_{n-1})}(t) \times M_{ba}^{n(l_1,\ldots,l_{n-1})}(s) \quad (6)$$

with

$$M_{ba}^{n(l_1,\ldots,l_{n-1})}(s) = m_{bl_{n-1}}(s)\, m_{l_{n-1}l_{n-2}}(s)\cdots m_{l_1 a}(s) = \exp\left(2\pi i \gamma_{n(l_{n-1},l_{n-2},\cdots,l_1)} s/N\right), \quad (7)$$

and

$$\gamma_{n(l_{n-1},l_{n-2},\cdots,l_1)} = \gamma_{bl_{n-1}} + \gamma_{l_{n-1}l_{n-2}} + \cdots + \gamma_{l_1 a}. \quad (8)$$

Due to the orthogonality of encoding functions $M_{ba}^{n(l_1,\ldots,l_{n-1})}(s)$, the pathway amplitudes $U_{ba}^{n(l_1,\ldots,l_{n-1})}(t)$ featured by the frequency of $\gamma_{n(l_{n-1},l_{n-2},\cdots,l_1)}$ can be obtained by performing an inverse fast Fourier transform (IFFT) of $U_{ba}(t,s)$.

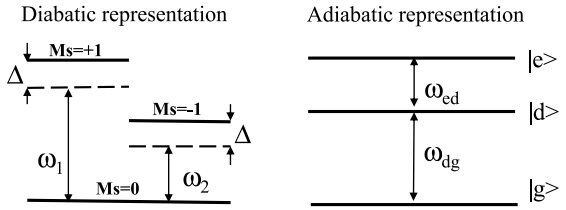

Fig. 1. Energy-level diagram of the NV center in diabatic and IA representations. The electronic spin-triplet states are labeled with $|M_s\rangle$, and the dressed states are denoted with $|g\rangle$, $|d\rangle$ and $|e\rangle$.

2.2. Diabatic and interaction adiabatic representations

A nitrogen–vacancy (NV) center is actually a spin defect consisting of a substitutional nitrogen impurity adjacent to a carbon vacancy in diamond. According to the electronic structure theory, its property is determined by six electrons, with two from the nitrogen atom, three from the carbon atoms surrounding the vacancy and one from the lattice [25–27]. The net spin is one due to the unpaired electron of the vacancy, leading to three energy levels with the magnetic quantum number M_s equal to 0, 1 or -1. As shown in Fig. 1, the two levels with $M_s = \pm 1$ are degenerate due to the axial symmetry, while the state $M_s = 0$ is energetically lower.

In the diabatic representation, the electronic spin ground states of an NV center in an external field B_z along the symmetry axis can be described by the following Hamiltonian [28]:

$$H = DS_z^2 + \gamma_e B_z S_z, \quad (9)$$

where $D = 2.87$ GHz is the so-called zero-field splitting [22], and the second Zeeman term $\gamma_e = 2.802$ MHz/G determines the eigenstates $|M_s\rangle$.

In experiment, two off-resonant continuous microwave driving fields are usually applied to transitions $|0\rangle \to |\pm 1\rangle$ at the same time. In the interaction picture, the Hamiltonian of the NV center driven by two microwaves with the same off-resonance Δ can be obtained by using rotating-wave approximation:

$$H_{NV} = H_a + H_b \quad (10)$$

with

$$H_a = \begin{bmatrix} \Delta + \gamma_e b & 0 & 0 \\ 0 & 0 & 0 \\ 0 & 0 & \Delta - \gamma_e b \end{bmatrix},$$

$$H_b = \begin{bmatrix} 0 & \frac{1}{2}\Omega_1(t) & 0 \\ \frac{1}{2}\Omega_1(t) & 0 & \frac{1}{2}\Omega_2(t) \\ 0 & \frac{1}{2}\Omega_2(t) & 0 \end{bmatrix}.$$

Here Ω_1 and Ω_2 are the Rabi frequencies of the two transitions. Then the Hamiltonian is transformed to eliminate its nonzero diagonal elements

$$H_I = e^{iH_a t}\cdot H_b \cdot e^{-iH_a t} = \frac{1}{2}\begin{bmatrix} 0 & \Omega_1(t)e^{i(\Delta+\gamma_e b)t} & 0 \\ \Omega_1(t)e^{-i(\Delta+\gamma_e b)t} & 0 & \Omega_2(t)e^{-i(\Delta-\gamma_e b)t} \\ 0 & \Omega_2(t)e^{i(\Delta-\gamma_e b)t} & 0 \end{bmatrix}. \quad (11)$$

The encoding in the diabatic representation is performed to this Hamiltonian.

In the following, we will introduce how to encode in the interaction adiabatic (IA) representation [14]. The time varying transformation that diagonalizes $H_{NV}(t)$ is $R_A(t)$, which links the dressed states and eigenstates $|M_s\rangle$. Then in the adiabatic representation, the evolution of the propagator becomes

$$\frac{dU'(t)}{dt} = \left[-iR_A^+(t) H_I(t) R_A(t) + \frac{dR_A^+(t)}{dt} R_A(t) \right] U'(t), \quad (12)$$

which corresponds to the new Hamiltonian

$$H'(t) = H_1(t) + H_2(t) = R_A^+(t) H_I R_A(t) + i \frac{dR_A^+(t)}{dt} R_A(t).$$

The first term shows the energy levels of the dressed states, while the second can be seen as the coupling between them. Then the Hamiltonian in the IA representation can be obtained by performing the following transformation:

$$H_{IA}(t) = R_I^+(t) H_2(t) R_I(t) = iR_I^+(t) \frac{dR_A^+(t)}{dt} R_A(t) R_I(t), \quad (13)$$

with

$$R_I(t) = \exp\left(-i \int_0^t H_1(t') dt' \right).$$

In Sec. 3, the control mechanisms are investigated in the diabatic and IA representations by encoding the Hamiltonians in Eqs. (11) and (13), respectively.

3. Mechanism analysis

3.1. Computation details

When the magnetic field $b = 0$, the eigenvalues of the Hamiltonian H_{NV} are $\lambda_0 = \Delta$ and $\lambda_\pm(t) = \frac{\Delta}{2} \pm \frac{\Omega_e(t)}{2}$, where $\Omega_e(t) = \sqrt{\Omega_1^2(t) + \Omega_2^2(t) + \Delta^2}$. The time varying transformation that diagonalizes $H_{NV}(t)$ is

$$R_A(t) = \begin{pmatrix} \sin\theta\sin\varphi & \cos\theta & \sin\theta\cos\varphi \\ -\cos\varphi & 0 & \sin\varphi \\ \cos\theta\sin\varphi & -\sin\theta & \cos\theta\cos\varphi \end{pmatrix}, \quad (14)$$

where the angles are defined by $\tan\theta(t) = \Omega_1(t)/\Omega_2(t)$ and $\tan 2\varphi(t) = \Omega_0(t)/\Delta$ with $\Omega_0(t) = \sqrt{\Omega_1^2(t) + \Omega_2^2(t)}$. The dressed states are

$$\begin{aligned} |g\rangle &= \sin\theta\sin\varphi\,|1\rangle - \cos\varphi\,|0\rangle + \cos\theta\sin\varphi\,|-1\rangle, \\ |d\rangle &= \cos\theta\,|1\rangle - \sin\theta\,|-1\rangle, \\ |e\rangle &= \sin\theta\cos\varphi\,|1\rangle + \sin\varphi\,|0\rangle + \cos\theta\cos\varphi\,|-1\rangle. \end{aligned} \quad (15)$$

In the IA representation, the Hamiltonian becomes

$$H_{IA}(t) = i \begin{pmatrix} 0 & \dot\theta\sin\varphi e^{-f_1(t)} & \dot\varphi e^{f_2(t)-f_1(t)} \\ -\dot\theta\sin\varphi e^{f_1(t)} & 0 & -\dot\theta\cos\varphi e^{f_2(t)} \\ -\dot\varphi e^{f_1(t)-f_2(t)} & \dot\theta\cos\varphi e^{-f_2(t)} & 0 \end{pmatrix} \quad (16)$$

with

$$f_1(t) = \left(\frac{i}{\hbar} \int_0^t \lambda_+(t') dt' \right),$$

$$f_2(t) = \left(\frac{i}{\hbar} \int_0^t \lambda_-(t') dt' \right).$$

When the magnetic field $b \neq 0$, it's difficult to get an analytical expression for the Hamiltonian in the IA representation. But we can obtain $H_{IA}(t)$ numerically according to the procedures listed in subsection 2.2.

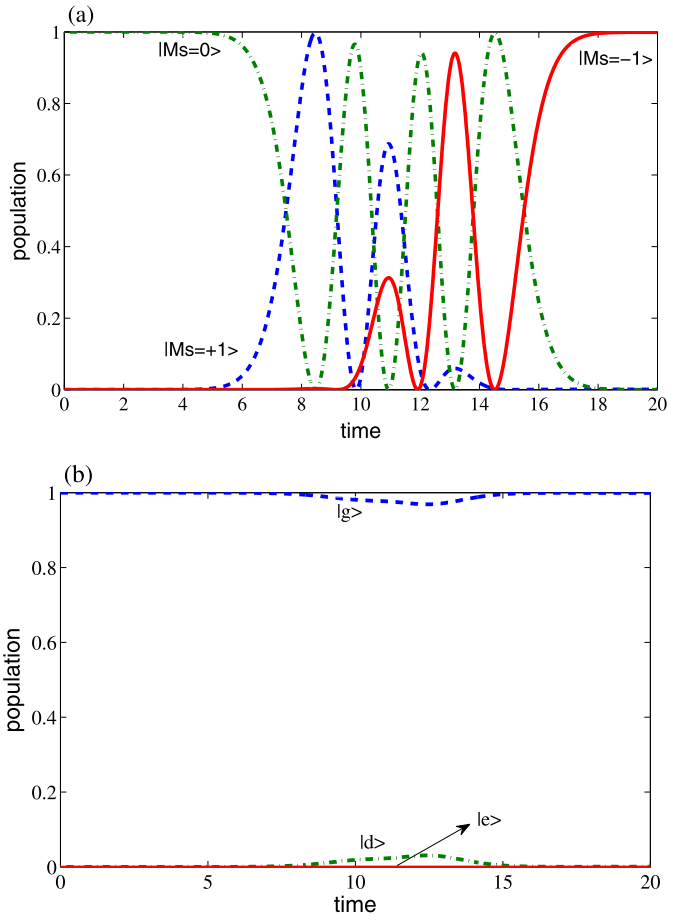

Fig. 2. The dynamics in the diabatic (panel (a)) and adiabatic basis (panel (b)). The parameter (in arbitrary units) are $A_m = 2.5$, $\Delta = 0$, $b = 0$, and $\sigma = 3$ μs.

The Rabi frequencies are defined by $\Omega_j(t) = A_m \exp\{-[(t - t_j)/\sigma]^2\}$ $(j = 1, 2)$, with $t_2 = t_1 + \sigma$, $t_1 = \frac{1}{2}T$ and $T = 20$ μs. In the following simulations, units of A_m, b and Δ are, respectively, atomic unit, G and MHz.

3.2. Numerical results

With parameter $A_m = 2.5$, $\Delta = 0$, $b = 0$, and $\sigma = 3$ μs, the population dynamics of the NV center are shown in Fig. 2 in two bases. In the diabatic basis (panel (a)), there is an overall transition from state $|Ms = 0\rangle$ to state $|Ms = -1\rangle$, but all states are involved in the dynamic evolution. In the adiabatic basis (panel (b)), almost all population remains in the initial state $|g\rangle$. Only a small amount of transition from $|g\rangle$ to $|d\rangle$ occurs in the dynamic process, while state $|e\rangle$ stays nearly unexcited. As seen in the left bottom panels of Figs. 3 and 4, pathways contributing to the dynamics in the two representations also show the difference. In Ref. [28], Xu et al. chose the dressed states $|g\rangle$ and $|d\rangle$ as a qubit, and found that their energies are insensitive to b, then eventually achieved a much longer coherence time in the subspace spanned by $|g\rangle$ and $|d\rangle$.

With other parameters adopted in this work, the general feature does not change. The dynamics in the adiabatic basis is much simpler than that in the diabatic basis, which can also be seen in the following mechanism analysis. The control mechanisms of the NV center with different parameters (*i.e.* Δ, b and A_m) are investigated by HE–OD in both diabatic and IA representations. The encoding matrix is the same for both representations:

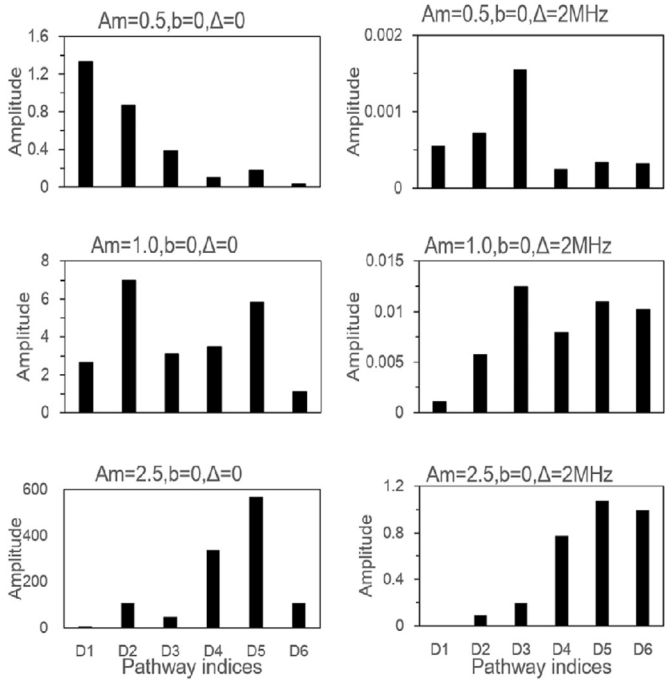

Fig. 3. Pathway amplitudes in the diabatic representation for detunings $\Delta = 0$ and $\Delta = 2$ MHz when magnetic field b is taken to be zero. Each bar indicates the contribution of a particular pathway. The horizontal axis labels the IFFT frequencies of U_{-10}, with notations D1, D2, D3, D4, D5, D6 labeling pathways $|0\rangle \to |-1\rangle$, $|0\rangle \to |1\rangle \to |0\rangle \to |-1\rangle$, $|0\rangle \to |-1\rangle \to |0\rangle \to |-1\rangle$, $|0\rangle \to |1\rangle \to |0\rangle \to |1\rangle \to |0\rangle \to |-1\rangle$, $|0\rangle \to |1\rangle \to |0\rangle \to |-1\rangle \to |0\rangle \to |-1\rangle$ ($|0\rangle \to |-1\rangle \to |0\rangle \to |1\rangle \to |0\rangle \to |-1\rangle$), and $|0\rangle \to |-1\rangle \to |0\rangle \to |-1\rangle \to |0\rangle \to |-1\rangle$, respectively.

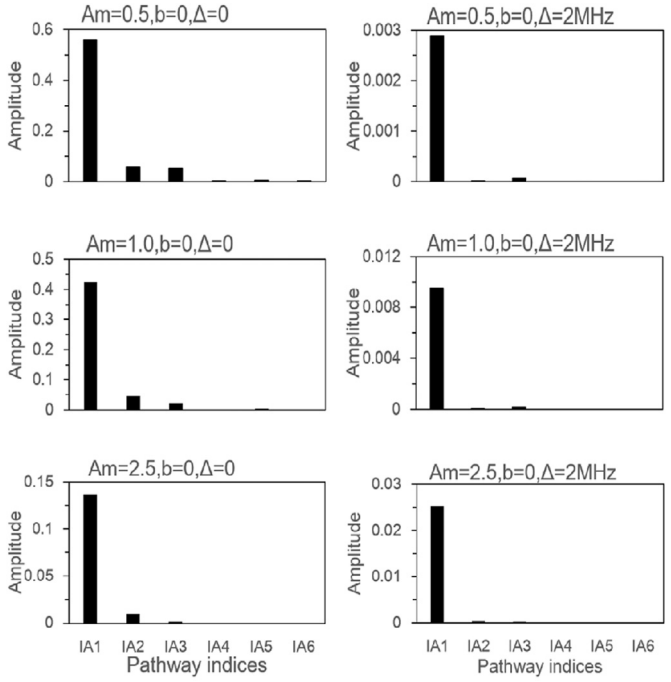

Fig. 4. Pathway amplitudes in the IA representation for detunings $\Delta = 0$ and $\Delta = 2$ MHz when magnetic field b is taken to be zero. Each bar indicates the contribution of a particular pathway. The horizontal axis labels the IFF frequencies of U_{gg}, with notations IA1, IA2, IA3 labeling pathways $|g\rangle \to |d\rangle \to |g\rangle$, $|g\rangle \to |d\rangle \to |g\rangle \to |d\rangle \to |g\rangle$ and $|g\rangle \to |d\rangle \to |e\rangle \to |d\rangle \to |g\rangle$, respectively. Notations IA4, IA5, IA6 are the high-order pathways, which are not specified here due to their negligible amplitudes. The fact that there are fewer pathways contributing to the dynamics in the IA representation indicates that this representation is more appropriate for mechanism analysis with these parameters.

$$\Gamma = \begin{pmatrix} 0 & 1 & 0 \\ 1 & 0 & 13 \\ 0 & 13 & 0 \end{pmatrix}.$$

The extracted amplitudes of significant pathways are shown in Figs. 3 and 4, respectively, for $\Delta = 0$ and $\Delta = 2$ MHz. There are fewer pathways contributing to the population transfer in the IA representation indicating that this representation is more appropriate for the mechanism analysis under our setting condition. The second-order pathway $|g\rangle \to |d\rangle \to |g\rangle$ always has the largest amplitude, which is consistent the dynamics shown in Fig. 2(b). In the diabatic representation, higher-order pathways will become dominant and the pathway amplitudes be larger with increased field intensity A_m for both the two cases $\Delta = 0$ and $\Delta = 2$ MHz. However, things are different in the IA representation. The pathway amplitudes become smaller for $\Delta = 0$ while larger for $\Delta = 2$ MHz with increased A_m. The trends of pathway amplitudes with increased field intensities can also be obtained by analyzing the corresponding Dyson terms. The simplest pathway $|0\rangle \to |-1\rangle$ in the diabatic representation is taken as example here.

The amplitude of pathway $|0\rangle \to |-1\rangle$ for $b = 0$ can be written as

$$\begin{aligned} U^1_{-1,0} &= \int_0^T \frac{1}{2} \cdot A_m \cdot \exp(-(\frac{t-t_2}{\sigma})^2) \cdot \exp(-i\Delta t)\, dt \\ &= \frac{1}{2} A_m \cdot \exp\left(-\frac{\sigma^2\Delta^2}{4} - i\Delta t_2\right) \\ &\quad \times \int_0^T \exp\left(-\frac{\left[t - \left(t_2 - \frac{i\sigma^2\Delta}{2}\right)\right]^2}{\sigma^2}\right) dt. \end{aligned} \tag{17}$$

It is obvious that the amplitude is proportional to A_m.

When the magnetic field $b \neq 0$, the pathway amplitude $U^1_{-1,0}$ changes differently when b increases under resonant and off-resonant conditions, as shown in Fig. 5. The expressions for $\Delta = 0$ and $b \neq 0$ are

$$U^1_{-1,0} = \int_0^T \frac{1}{2} \cdot A_m \cdot \exp(-(\frac{t-t_2}{\sigma})^2) \cdot \exp(i \cdot \gamma_e \cdot b \cdot t) \cdot dt. \tag{18}$$

With the chosen parameters of driving fields, it becomes

$$\begin{aligned} U^1_{-1,0} &= \int_0^{20} \frac{1}{2} \cdot 1.0 \cdot \exp(-(\frac{t-13}{3})^2) \cdot \exp(i \cdot \gamma_e \cdot b \cdot t) \cdot dt \\ &= \frac{3}{2} \cdot \sqrt{\pi} \cdot \exp(36.4bi - 17.64b^2), \end{aligned} \tag{19}$$

then

$$\left|U^1_{-1,0}\right| = \frac{3}{2} \cdot \sqrt{\pi} \cdot \exp(-17.64b^2).$$

For $\Delta = 2$ MHz and $b \neq 0$, the pathway amplitude is

$$\begin{aligned} U^1_{-1,0} &= \int_0^T \frac{1}{2} \cdot A_m \cdot \exp(-(\frac{t-t_2}{\sigma})^2) \cdot \exp\left[i \cdot (\gamma_e \cdot b - \Delta) \cdot t\right] \cdot dt \\ &= \frac{3}{2} \cdot \sqrt{\pi} \cdot \exp(13\,(2.8 \cdot b - 2)\, i - \frac{9}{4}\,(2.8 \cdot b - 2)^2), \end{aligned} \tag{20}$$

then

$$\left|U^1_{-1,0}\right| = \frac{3}{2} \cdot \sqrt{\pi} \cdot \exp(-\frac{9}{4}\,(2.8 \cdot b - 2)^2).$$

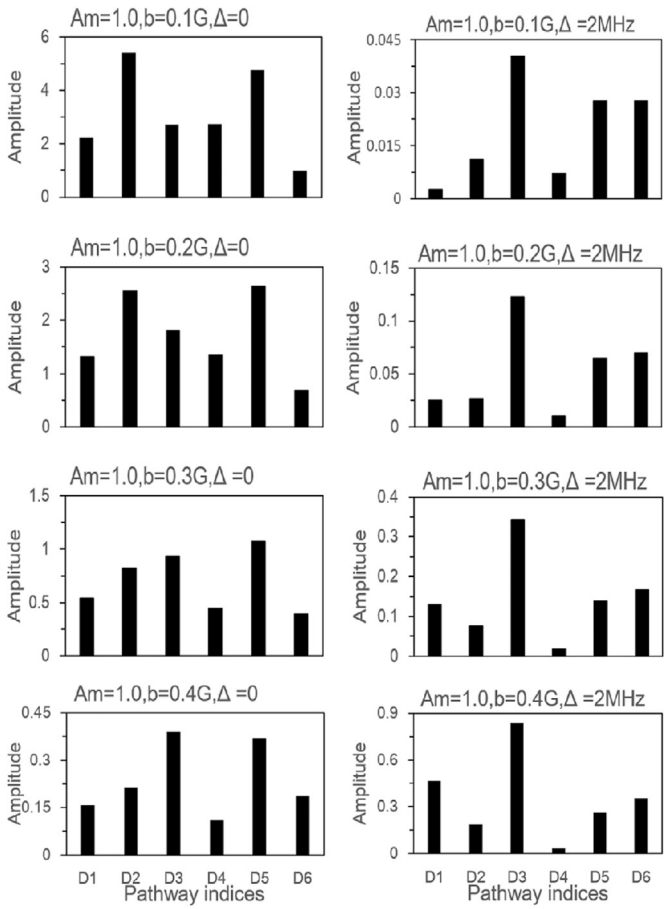

Fig. 5. Significant pathways for different magnetic fields b and detunings Δ in the diabatic representation. Parameters of driving fields are $t_1 = 10$ μs, $t_2 = 13$ μs, $A_m = 1.0$ and $\sigma = 3$ μs. The notations in the horizontal axis are the same as in Fig. 3.

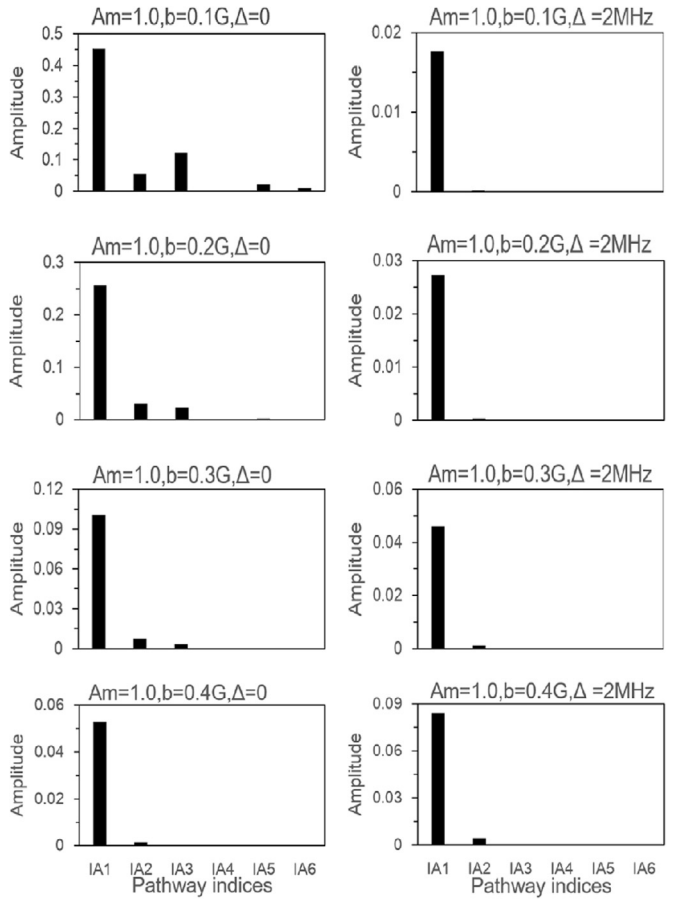

Fig. 6. Significant pathways for different magnetic fields b and detunings Δ in the IA representation. Parameters of driving fields are $t_1 = 10$ μs, $t_2 = 13$ μs, $A_m = 1.0$ and $\sigma = 3$ μs. The notations in the horizontal axis are the same as in Fig. 4.

It can be seen that the trends of $\left|U^1_{-1,0}\right|$ are opposite for cases of $\Delta = 0$ and $\Delta = 2$ MHz.

4. Conclusions and discussions

The control mechanism of the nitrogen–vacancy (NV) center system is investigated with the HE–OD method in both diabatic and IA representations. The experimental parameters are used in our simulations. Since in the experiment the two lowest dressed states are employed as a qubit, the IA representation is more suitable for mechanism analysis. This is proved that the fact that there is only one pathway $|g\rangle \to |d\rangle \to |g\rangle$ dominating the dynamics in the adiabatic basis while more pathways contribute in the dynamics in the diabatic basis. Different parameters (*i.e.* driving fields, magnetic fields, detunings) are adopted. It is found that the tendencies of pathway amplitudes when one of the parameters changes are different under various conditions, which can be analyzed from the corresponding Dyson terms.

The underlying control mechanisms extracted from HE–OD analysis indeed give hints on how to improve the control effect. For example, in Figs. 3 and 4, with the same parameters $A_m = 2.5$, $b = 0$, $\Delta = 0$, the pathway amplitudes demonstrate different behavior in the two representations. In the diabatic representation, besides the initial state $|0\rangle$ and target state $|-1\rangle$, state $|-1\rangle$ is also involved in pathways D2, D4 and D5, whose amplitudes are large. However, in the IA representation, significant pathways IA1 and IA2, which involve states $|g\rangle$ and $|d\rangle$, have relative larger amplitude, while the pathway IA3 involving an additional state $|e\rangle$ has a much smaller amplitude. These facts indicate that the two states $|g\rangle$ and $|d\rangle$ are preferable to be employed as a qubit than $|0\rangle$ and $|-1\rangle$ under the current Hamiltonian and parameters, which is consistent with Ref. [28]. The population leakage from the two states of a qubit to another state will reduce the fidelity. Therefore, the further improvement of the fidelity can be realized by making the pathway amplitudes involving additional states approach zero.

The environmental effects in NV-center systems are mainly from the surrounding ^{13}C nuclear spin bath fluctuations, which can be described by an effective weak random magnetic field b with time correlation [29]. Figs. 5 and 6 show different tendencies of quantum pathway amplitudes with magnetic fields in the two representations: the relative ratios of different pathways in the IA representation vary less than those in the diabatic representation. The results indicate that states $|g\rangle$ and $|d\rangle$ in the IA representation perform much better as two states of a qubit than the state pair $|0\rangle$ and $|-1\rangle$, which is also consistent with the conclusions in Ref. [28].

Acknowledgements

The authors acknowledge support by the National Natural Science Foundation of China (Grants No. 61720106009, No. 61773359, No. 61403362, No. 61374091, and No. 61473199). F. Shuang thanks the Leader talent plan of the Universities in Anhui Province and the CAS Interdisciplinary Innovation Team of the Chinese Academy of Sciences for financial support.

References

[1] H. Rabitz, R. de Vivie-Riedle, M. Motzkus, K. Kompa, Science 288 (2000) 824.

[2] J.L. Herek, W. Wohlleben, R.J. Cogdell, D. Zeidler, M. Motzkus, Nature 417 (2002) 533.
[3] H.M. Wiseman, A.C. Doherty, Phys. Rev. Lett. 94 (2004) 070405.
[4] H. Mabuchi, Phys. Rev. A 78 (2008) 032323.
[5] J. Zhang, Y.X. Liu, F. Nori, Phys. Rev. A 79 (2009) 052102.
[6] Y. Silberberg, Annu. Rev. Phys. Chem. 60 (2009) 277.
[7] J. Zhang, Y.X. Liu, R.B. Wu, C.W. Li, T.J. Tarn, Phys. Rev. A 82 (2009) 022101.
[8] G.G. Gillett, R.B. Dalton, B.P. Lanyon, M.P. Almeida, M. Barbieri, G.J. Pryde, J.L. O' Brien, K.J. Resch, S.D. Bartlett, A.G. White, Phys. Rev. Lett. 104 (2009) 080503.
[9] C. Altafini, F. Ticozzi, IEEE Trans. Autom. Control 57 (2012) 1898–1917.
[10] C. Brif, M.D. Grace, M. Sarovar, K.C. Young, New J. Phys. 16 (2014) 065013.
[11] S.J. Glaser, U. Boscain, T. Calarco, C.P. Koch, Walter Köckenberger, R. Kosloff, I. Kuprov, B. Luy, S. Schirmer, T. Schulte-Herbrüggen, D. Sugny, F.K. Wilhelm, Eur. Phys. J. D 69 (2015) 279.
[12] F. Gao, R. Rey-de-Castro, Y. Wang, H. Rabitz, F. Shuang, Phys. Rev. A 93 (2016) 053407.
[13] A. Mitra, H. Rabitz, Phys. Rev. A 67 (2003) 033407.
[14] A. Mitra, I.R. Sola, H. Rabitz, Phys. Rev. A 67 (2003) 043409.
[15] A. Mitra, H. Rabitz, J. Chem. Phys. 125 (2006) 194107.
[16] A. Mitra, H. Rabitz, J. Chem. Phys. 128 (2008) 044112.
[17] A. Mitra, I.R. Sola, H. Rabitz, Phys. Rev. A 77 (2008) 043415.
[18] R. Rey-de-Castro, H. Rabitz, Phys. Rev. A 81 (2010) 063422.
[19] R. Rey-de-Castro, R. Cabrera, D.I. Bonder, H. Rabitz, New J. Phys. 15 (2013) 025032.
[20] R. Rey-de-Castro, Z. Leghtas, H. Rabitz, Phys. Rev. Lett. 110 (2013) 223601.
[21] F. Gao, R. Rey-de-Castro, A.M. Donovan, J. Xu, Y. Wang, H. Rabitz, F. Shuang, Phys. Rev. A 89 (2014) 023416.
[22] M. Doherty, N. Manson, P. Delaney, F. Jelezko, J. Wrachtrup, L. Hollenberg, Phys. Rep. 528 (1) (2013) 1–45.
[23] G. Balasubramanian, P. Neumann, D. Twitchen, et al., Nat. Mater. 8 (2009) 383.
[24] G.D. Fuchs, V.V. Dobrovitski, D.M. Toyli, F.J. Heremans, D.D. Awschalom, Science 326 (2009) 1520.
[25] R. Schirhagl, K. Chang, M. Loretz, C.L. Degen, Annu. Rev. Phys. Chem. 65 (2014) 83–105.
[26] I. Aharonovich, S. Castelletto, D. Simpson, C.H. Su, A.D. Greentree, S. Prawer, Rep. Prog. Phys. 74 (2011) 076501.
[27] J.R. Maze, A. Gali, E. Togan, Y. Chu, A. Trifonov, E. Kaxiras, M.D. Lukin, New J. Phys. 13 (2) (2010) 025025.
[28] X. Xu, Z. Wang, C. Duan, P. Huang, P. Wang, Y. Wang, X. Kong, N. Xu, F. Shi, X. Rong, J. Du, Phys. Rev. Lett. 109 (2012) 070502.
[29] G. de Lange, Z.H. Wang, D. Rist, V.V. Dobrovitski, R. Hanson, Science 330 (2010) 60.